Synthetic silico-metallic particles-SSMMP-Ni and SSMMP-Ni-IL: CO2 capture and utilization

Daniela Rodrigues, Julia Wolf, Barbara Polesso, Pierre Micoud, Christophe Le Roux, Franciele Bernard, François Martin, Sandra Einloft

Synthetic silico-metallic particles- SSMMP-Ni and SSMMP-Ni-IL: CO_2 capture and utilization

Daniela Rodrigues[1,3], Julia Wolf[2], Barbara Polesso[1], Pierre Micoud[3], Christophe Le Roux[3], Franciele Bernard[2], François Martin[3], Sandra Einloft[1,2]

[1]*Post-Graduation Program in Materials Engineering and Technology, Pontifical Catholic University of Rio Grande do Sul – PUCRS, Brazil.*

[2]*School of Technology, Pontifical Catholic University of Rio Grande do Sul PUCRS, Brazil.*

[3]*GET/OMP (CNRS, UT3PS, IRD, CNES), Université de Toulouse, ERT Géomatériaux, (Toulouse) France*

Abstract

Synthetic silico-metallic mineral particles (SSMMP) containing different amounts of Ni (SSMMP-Ni) and SSMMP-Ni functionalized with different IL (SSMMP-Ni-IL) were obtained and successfully used as solid adsorbents for CO_2 sorption, CO_2/N_2 separation and highly recyclable heterogeneous catalysts active in the synthesis of different cyclic carbonates using CO_2 as a starting reagent. Samples were characterized by infrared spectroscopy (FTIR), RAMAN spectroscopy, X-ray diffraction (XRD), thermal analysis (TGA), specific surface area measurements (BET) and scanning electron microscopy (SEM). Samples containing IL demonstrated high CO_2 capture capacity (1.18-1.91 mmol CO_2/g adsorbent - 1bar CO_2), CO_2 selectivity (7.5-14.7) and stability. As catalysts, SSMMP-Ni 50% achieved a yield of 93.3% in propylene carbonate production (20 bar, 100ºC and 7h) and constant yield up to 10 cycles. These materials are easy to synthesize, with low energy demand, high stability and versatile to be used as adsorbent in CO_2 capture and catalyst for CO_2 transformation.

Keywords: CO_2/N_2 separation; nickel synthetic silico-metallic mineral particles; CO_2 capture; CO_2 utilization; solid sorbents; heterogeneous catalysis

1. Introduction

The need to reduce the amount of CO_2 emitted into the atmosphere by the anthropogenic burning of fossil fuels is urgent. Energy production is majoritarian by fossil fuel and the prediction that it will continue in the next years is clear [1,2]. Mitigating CO_2 emissions into the atmosphere is an imperative discussion to be

continued by heads of state and a huge challenge for scientists [3]. The portfolio of technologies available to reduce CO_2 concentrations in the atmosphere during this transition period of carbon-based to zero-carbon energy production includes CO_2 capture, utilization, and storage as mature options. Carbon capture and storage (CCS) aims to capture CO_2 before it is released into the atmosphere. After capturing the CO_2, it is separated from the other gases and transported to geological storage. Among the available techniques, capturing CO_2 from gaseous effluents after fuel combustion is considered advantageous due to its integration into existing industrial facilities [2,4–7]. Besides being the benchmark technology, chemical adsorption by aqueous solution amines presents some drawbacks, such as high volatility and low thermal stability, high cost of amine regeneration, degradation of amines and equipment corrosion [2]. Thus, the development of materials with high CO_2 capture efficiency and selectivity, low cost, and recyclability are urgent [8].

Problems related to CO_2 storage (such as the limited capacity for CO_2 geological storage, uncertainties regarding safety and storage time, and the lack of financial incentives), brought to light carbon capture and utilization technologies (CCU) [5,9]. CCU presents the possibility of transforming residual CO_2 into a starting reagent in the production of industry-valuable chemical products. Cyclic carbonates can be used in industry as electrolytes in lithium batteries, monomers in polycarbonate synthesis, aprotic polar solvents, and reagents in the pharmaceutical industry and agricultural chemicals production [5,9,10]. However, CO_2 low reactivity and high thermodynamic stability demand the use of catalysts to the reaction efficiently occur with low energy expenditure. Homogeneous and heterogeneous catalysts are described for use in cyclic carbonates synthesis, including metallic salts [11], metallic oxides [12,13], ionic liquids [14], organic bases [15,16], metallic complexes [17,18] and metal-organic frameworks MOFs [19]. Homogeneous catalysts present good catalytic activity but the difficulty and cost of separating the product and catalyst are undesirable. Heterogeneous catalysts have drawbacks such as low catalytic activity, selectivity, and catalyst recyclability. Yet, the high energy demand for catalyst manufacture is an important issue [4,20]. In this scenario, it is imperative to continue the search for new efficient, recyclable, and low production cost heterogeneous catalysts.

The use of ionic liquids (IL) in CO_2 capture and transformation has been widely explored. In the first, as an alternative to amine solutions and in the second as homogeneous catalysts in carbonates synthesis. IL exhibits properties such as good

thermal stability, high ionic conductivity, good solubility, wide electrochemical potential window, high synthetic flexibility, non-flammable, recyclable and low vapor pressure and is classified as a green solvent [21–23]. However, the high viscosity of ILs results in low CO_2 diffusion and, consequently, low CO_2 sorption rates, making their use inconvenient for CO_2 capture [24]. An alternative to solve the inconvenience both as a homogeneous catalyst and for CO_2 absorption (high viscosity) is the use of IL supported on solid materials. Among the materials used as support are organic and inorganic polymers, silicas, nanoparticles, oxides, resins, MOFs and zeolites [2,7,10,24–31]. Silica-based materials are interesting to be used as support, they have many silanol groups (-SiOH) on their surface facilitating functionalization in addition to the affinity for the CO_2 [32]. SSMMP are synthetic talc precursor particles having a structure described as “nano-talc entities”. SSMMP are formed by 2-3 Mg octahedra with 3-4 Si tetrahedra distributed in the lower and upper part of the Mg octahedral “sheet”. After hydrothermal treatment, these “nano-talc entities” produce synthetic talc, stacked lamellae composed of octahedral sheets of Mg sandwiched by two tetrahedral sheets of Si bonded together by weak Van der Waals forces [33,34]. The main advantage of using SSMMP compared to synthetic talc is a large number of reactive groups (-SiOH and -MgOH) on the entire surface (against only 10% of the surface of synthetic talc), providing an excellent interaction with CO_2 and potentially synergistic effect with the IL [7,34,35]. Yet, the elimination of the step with the highest energy expenditure in the synthesis (hydrothermal treatment) makes these materials low-cost and easy to synthesize [7]. Partial and/or total Mg cation exchange by Ni and other divalent cations in the octahedral layer of synthetic talc was revisited and the application possibilities of these materials were also explored (Martin et al., 2019).

The synthesis of SSMMP functionalized with IL, from a fast, one-step, low-energy method using only water as a solvent for dissolving the reagents places this material as a candidate for different applications [37]. SSMMP can be used as support materials for IL and further applied as solid materials for heterogeneous catalysis, heavy metal sorption and selective gas sorption [7]. Recently our group proved that Mg-based SSMMP can be used as a selective sorbent for CO_2/N_2 separation [7].

In this work, the synthesis and characterization of SSMMP with 50 and 100% of Ni replacing Mg were described. Yet, ammonium and imidazolium-based IL (20%) were supported by replacing Si during the synthesis. Obtained materials were further tested as solid adsorbents in CO_2 capture at 25ºC, at CO_2 equilibrium pressures of 1-30 bar,

and as selective adsorbents for CO_2 in CO_2/N_2 gas mixtures. Thinking in the possibility of having CO_2 capture and transformation steps in the same place, SSMMP were also tested as heterogeneous recyclable catalysts in the CO_2 cycloaddition reactions in epoxides (10-30 bar, 60-110ºC and 4-8 hours).

2. Experimental

2.1. Materials

Sodium metasilicate pentahydrate ($Na_2SiO_3.5H_2O$, Sigma-Aldrich), sodium acetate (CH_3COONa, Sigma-Aldrich), magnesium acetate tetrahydrate ($(CH_3COO)_2Mg.4H_2O$, Sigma-Aldrich), acetic acid (CH_3COOH, Sigma-Aldrich), nickel acetate tetrahydrate ($Ni(CH_3COO)_2.4H_2O$, Sigma-Aldrich), 1-triethoxysilylpropyl-n.n.n-methylimidazolium chloride [IMI-Cl-silane], 1-trimethoxysilylpropyl-n.n.n-trimethylammonium chloride ([AMO-Cl-Silane], Gelest), sodium bromide (NaBr, Sigma-Aldrich), sodium iodide (NaI, Sigma-Aldrich), propylene epoxide (Sigma-Aldrich), styrene epoxide (Sigma-Aldrich), 1,2-epoxybutane (Sigma-Aldrich), epichlorohydrin (Sigma-Aldrich), tetrabutylammonium bromide (TBAB, Sigma-Aldrich) and CO_2 (Air Liquide, 99.998%). All reagents were used as purchased without further purification.

Table 1- Simplified scheme of samples synthesis reactions

Entry	Sample	Reaction equation
1	**ST-Ni 50%**	4 [Na_2SiO_3] + 1.5 [$Ni(CH_3COO)_2$] +1.5 [$Mg(CH_3COO)_2$] +2 CH_3COOH → ***ST-Ni 50%*** + 8 CH_3COONa
2	**SSMMP-Ni 50%**	4 [Na_2SiO_3] + 1.5 [$Ni(CH_3COO)_2$] +1.5 [$Mg(CH_3COO)_2$] +2 CH_3COOH → ***SSMMP-Ni 50%*** + 8 CH_3COONa
3	**SSMMP-Ni 100%**	4 [Na_2SiO_3] + 3 [$Ni(CH_3COO)_2$] +2 CH_3COOH → ***SSMMP-Ni 100%*** + 8 CH_3COONa
4	**SSMMP-Ni 50%- IL***	3.2 [Na_2SiO_3] +0.8 ***IL-silane***+ 1.5 [$Ni(CH_3COO)_2$] +1.5 [$Mg(CH_3COO)_2$] +2 CH_3COOH → ***SSMMP-Ni 50% - IL*** + 8 CH_3COONa

*IL = AMO-Br, AMO-Cl, AMO-I, IMI-Br, IMI-Cl and IMI-I

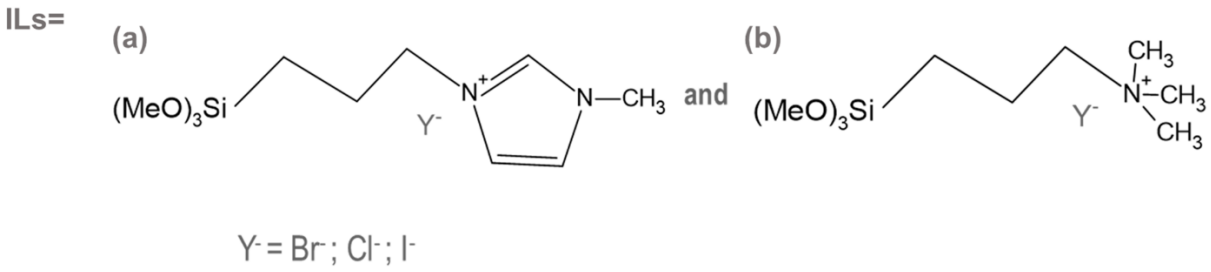

Figure 1- Structure of the ionic liquids functionalizing the SSMMP-Ni 50%. (a) [IMI-Y-Silane] and (b) [AMO-Y-Silane]

2.2. Synthetic talc synthesis

Synthetic talc with 50% Mg substituted by Ni (ST-Ni 50%) was synthesized using a protocol well described in the literature [33,38]. Talc synthesis was carried out in two stages: the first with the mixture of two solutions, a Si precursor, prepared from 0.2 mol of $Na_2SiO_3.5H_2O$ dissolved in 200 mL of purified water, and another precursor solution of Mg and Ni, prepared from 0.075 mol of $Mg(CH_3COO)_2.4H_2O$, 0.075 mol of $Ni(CH_3COO)_2.4H_2O$ and 0.1 mol of CH_3COOH dissolved in 300 mL of purified water. The second stage consists of the hydrothermal treatment of this mixture in an autoclave for 6 hours, at 300ºC, reaching a pressure of 85 bar. The talc gel obtained after hydrothermal treatment is washed and centrifuged to remove the sodium acetate, and dried in an oven at 100ºC. The equation and the synthesis process of ST-Ni-50% are represented in Table 1 (entry 1) and Figure 2.

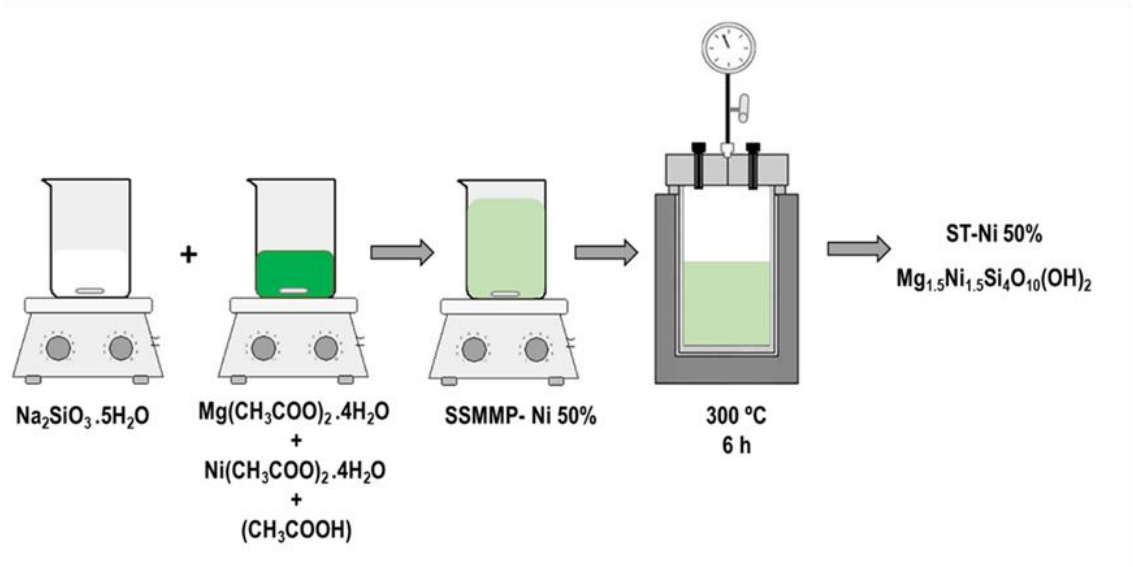

Figure 2- Schematic representation of the synthesis of ST-Ni 50%

2.3. Synthesis of SSMMP and SSMMP-IL

Synthetic silico-metallic mineral particles (SSMMP) synthesis was recently described by our group [7]. The SSMMP containing Ni in substitution of 50% or 100% of the octahedral Mg (SSMMP-Ni 50% and SSMMP-Ni 100%, respectively) were synthesized in a similar way to the first step of the synthesis of ST-Ni 50% (described in the previous topic 2.2, without supplementary addition of CH_3COONa in the Si precursor solution), with the exception for the synthesis of SSMMP-Ni 100% for which $Mg(CH_3COO)_2$ is replaced by $Ni(CH_3COO)_2$. After mixing the precursor solutions of Si, Mg and Ni, the formed precipitate was washed with water and centrifuged until the complete removal of sodium acetate. Finally, the SSMMP-Ni X% were oven dried for approximately 24 hours at 100ºC. The formation reactions of SSMMP-Ni 50% and SSMMP-Ni 100% are shown in Table 1 (entries 2 and 3).

The synthesis of the SSMMP-Ni 50%-IL was performed by adapting the synthesis method described by Dumas (2013a). The ILs [IMI-Cl-Silane] and [AMO-Cl-Silane] were diluted in purified water and the Cl^- anion was exchanged for Br^- and I^- anions using NaBr and NaI, respectively, resulting in ILs (IMI-Br, IMI-I, AMO-Br and AMO-I) as shown in Figure 1. The obtained ILs were mixed with the first solution of $Na_2SiO_3.5H_2O$ from formation synthesis of the SSMMP-Ni 50% following the same steps previously described for the synthesis of the SSMMP-Ni 50%, forming the samples named: SSMMP-Ni 50%-IMI Br, SSMMP-Ni 50%-IMI I, SSMMP-Ni 50%-AMO Br and SSMMP-Ni 50%-AMO I. The formation reaction of the SSMMP-Ni 50%-IL is represented in Table 1 (entry 4). In a typical SSMMP-Ni50% IL synthesis, the anion exchange was first performed using 0.08 mol of ILs (IMI-Cl-Silane or AMO-Cl-Silane) and 0.08 mol of the elected salt (NaBr or NaI) diluted in 100 mL of purified water, under constant stirring for 1 hour at room temperature. After the anion exchange, the IL-containing solution is mixed with a Si precursor solution (0.32 mol of $Na_2SiO_3.5H_2O$ dissolved in 300 ml of purified water). Finally, the solution containing the Si precursor and the IL is poured over the precursor solution of Mg and Ni (0.15 mol of $Mg(CH_3COO)_2.4H_2O$ and 0.15 mol of $Ni(CH_3COO)_2.4H_2O$ dissolved in 400 ml of purified water). The resulting precipitate is then centrifuged, washed with water and dried in an oven at 100°C.

2.4. Materials characterization

Perkin-Elmer FT-IR Spectrum 100 spectrometer in the range of 4000 cm^{-1} to 600 cm^{-1} was used to perform Fourier transform infrared spectroscopy (FT-IR). Confocal Raman microscopy system alpha300 R access from WiTec GmbH, equipped with a UHTS 300 spectrophotometer with a diffraction grating of 600g/mm BLZ=500 nm and using a He-Ne laser was used to obtain RAMAN spectrograms. Thermogravimetric analyses (TGA) were obtained using a TA Instrument SDT-Q600. The temperature range was set at 25°C–900°C with a heating rate of 20°C/min, under nitrogen atmosphere. The specific surface areas were obtained using Brunauer-Emmett–Teller (BET) method. The nitrogen adsorption-desorption isotherm was obtained using NOVA 4200 High Speed at liquid nitrogen temperature. X-ray diffraction (XRD) analyses were performed on disoriented powders, using a Bruker D8 Advance diffractometer operating under the reflection of the $CuK\alpha_{1+2}$ radiation (λ = 1.5418 Å), $K\alpha_2$ being subtracted with Bruker Diffrac. Eva software for figures. XRD patterns were collected over the 2-80°2θ range, using 0.4 s counting time per 0.01°2θ step at room temperature. The powdered talc skeletal density (ρs) was measured at 25°C using an Ultrapycnometer 1000 - Quantachrome Corporation pycnometer using ultra-high purity helium (Air Liquide / 99.999%). A field emission scanning electron microscope (FESEM) Inspect F50 equipment (FEI Instruments) was used to assess particle morphology.

2.5. CO_2 sorption capacity

CO_2 sorption capacity was evaluated using well-described procedures [39,40]. The pressure decay technique reported by KOROS and PAUL was used to perform the tests Koros & Paul (1976), using an equilibrium cell equipped with two chambers (one being a gas chamber and the other a sorption chamber). Sorption tests were carried out in triplicates at a constant temperature of 25°C using CO_2 at equilibrium pressures of 1, 10, and 30 bar and sample mass of 0.6 to 0.7g. Before each test, the samples were placed in an oven remaining 1h at 100°C. Ten cycles of CO_2 sorption/desorption were performed to corroborate sample stability.

2.6. CO_2 selectivity in CO_2/N_2 mixtures

CO_2 selectivity was performed with a mixture with a composition of 15:85 (v/v) of CO_2/N_2 using the same CO_2 sorption system described above [42,43] CO_2 selectivity tests was performed at 20 bar of equilibrium pressure, and 25 ºC of temperature, in

triplicate. For selectivity determination, two gas samples are taken from the system after the mixture pressure reaches equilibrium and injected into a gas chromatograph (GC) (Shimadzu GC-14B) equipped with a thermal conductivity detector to obtain the gaseous composition of the non-adsorbed mixture allowing the selectivity calculation as described in detail by Azimi and Mirzaei (2016).

$$S = \frac{{}^{X_{CO_2}}/_{Y_{CO_2}}}{{}^{X_{N_2}}/_{Y_{N_2}}} \quad (1)$$

The selectivity CO_2/N_2 is obtained using equation 1, where X_{CO2} and X_{N2} correspond to the molar fractions of CO_2 and N_2 sorbed by the sample, and Y_{CO2} and Y_{N2} are the molar fractions of CO_2 and N_2 present in the gas phase, respectively [7,42].

2.7. Cyclic carbonates synthesis

The synthesis of cyclic carbonates was carried out in a 120 mL titanium autoclave reactor. The system temperature is controlled by a thermocouple connected to a temperature controller. The reactor is charged with 0.1 mol of propylene oxide and 0.2 g of catalyst. For the reactions carried out using a cocatalyst TBAB (0.6 mol% of EP) was added. The reactor was closed, pressurized with different CO_2 pressures (10-30 bar) and heated (30-120 ºC). The temperature was kept constant for a predetermined time (2-7 hours). After each reaction, the reactor was slowly cooled and depressurized. The catalyst was separated from the reaction product by centrifugation. The reaction product was treated under vacuum and heated to remove any remaining unreacted propylene oxide. The final product was analyzed using a Shimadzu GC-14B gas chromatograph, equipped with a flame ionization detector (FID) and an SH-Rtx-5 column (30 m × 25 mm × 25 mm). A calibration curve with propylene carbonate as the internal standard and ethyl ether as solvent was previously constructed and used to determine reaction selectivity.

For cyclability tests, the catalyst was separated from the reaction product, washed with distilled water, centrifuged and dried in an oven at 100ºC for approximately 2 hours.

After drying, the catalyst was ready to be reused in the next cycle, with the addition of cocatalyst TBAB (0.6 mol% of EP).

3. Results and discussion

FTIR

ST-Ni 50%, SSMMP-Ni 50%, SSMMP-Ni 50%-AMO Br and SSMMP-Ni 50%-IMI Br FTIR spectra are presented in Figure 3, (a-d), respectively. For all samples, characteristic bands are seen at 3650 cm^{-1} attributed to (-OH) stretching vibration of the Mg_3-OH and Ni_3-OH, at 1023 cm^{-1} to symmetric stretching of Si-O-Si and Si-O, at 678 cm^{-1} to the overlapping of Ni-O and Si-O, and the OH groups deformation, and at 473 cm-1, related to the stretching vibration of Si-O-Si and the -OH groups [44–51]. The broad band at 3600-2800 cm^{-1} is attributed to the water hydroxyl group (-OH) confirmed by the characteristic band at 1635 cm^{-1} [52,53]. For SSMMP-Ni 50%-IMI Br (Figure 3, d), two characteristic bands are observed in the region of 1572 cm^{-1} and 1492 cm^{-1}, related to the C=C stretch bond of the imidazolium ring present in the ILs cation. The bands located at 1380 cm^{-1} and 1166 cm^{-1} are attributed to C-H bonds of the IL aliphatic chain and the Si-C, respectively [54,55]. SSMMP-Ni 50%-AMO Br (Figure 3, c) evidenced the bands at 1476 cm^{-1} and 1418 cm^{-1} related to CH_2 bond deformation [53,56]

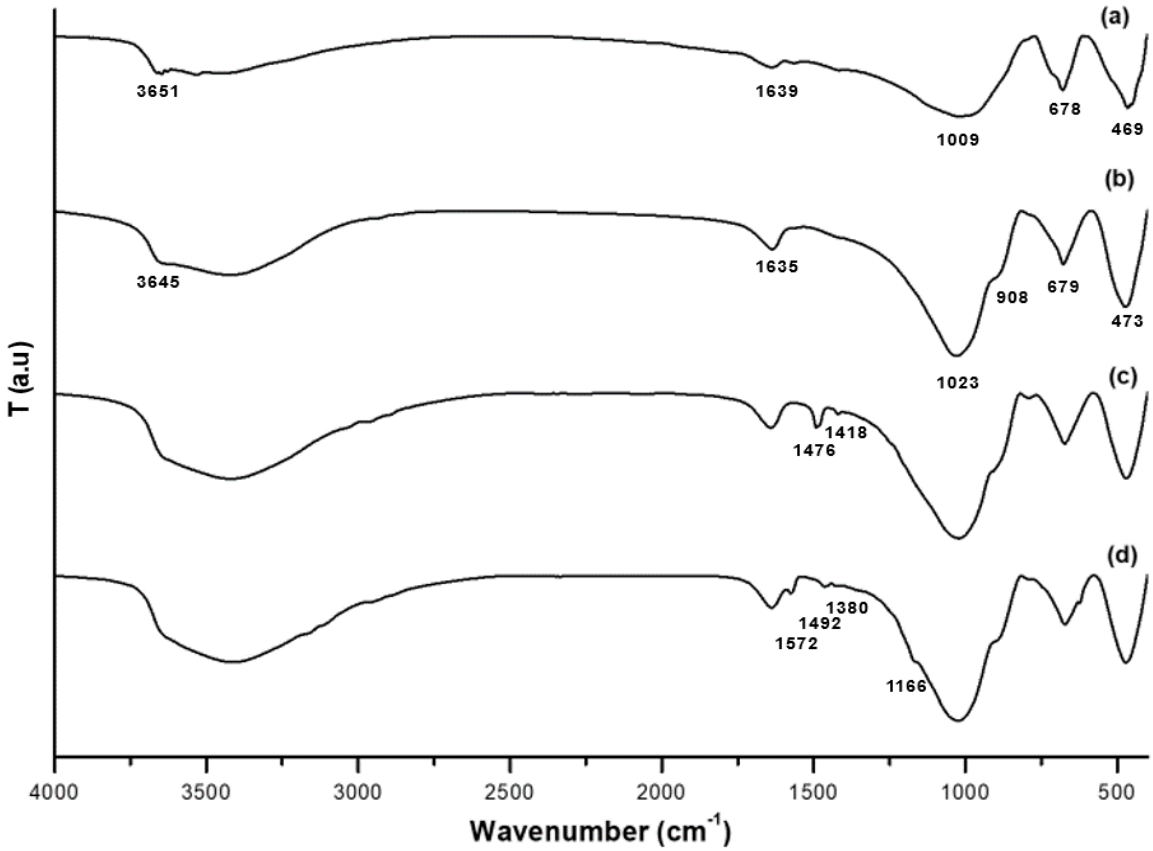

Figure 3- FTIR of samples (a) ST-Ni 50%, (b) SSMMP-Ni 50%, (c) SSMMP-Ni 50%-AMO Br and (d) SSMMP-Ni 50%-IMI Br

RAMAN

Figure 4 presents Raman spectra of SSMMP-Ni 50% and SSMMP-Ni 50%-IL. For all pristine and IL-functionalized samples a band near the 675 cm^{-1}, attributed to the symmetrical Si-O-Si elongation mode is observed [7,57]. For SSMMP-Ni 50%-IL (Figure 4, b-e), new bands appeared in the region of 2902 and 2990 cm^{-1}, characteristic of the CH_2- and CH_3- bonds stretching vibrations present in the side chains of the imidazolium and ammonium cations [7,58,59]. The bands between 900 and 1000 cm^{-1} are attributed to C-C bonds stretching vibrations of the cation side chains. For samples containing the ammonium cation (Figure 4, b and c), the bands at 1339 cm^{-1}, 1417cm^{-1} and 1560 cm^{-1} are attributed to C-N, CH_2- and CH_3- bond asymmetric stretching vibration, and CH_2-N bond vibration, respectively [59]. For samples containing the imidazolium cation, bands in the same region (between 1326 and 1530 cm^{-1}) were observed and attributed to in the plane asymmetric stretching vibrations of imidazolium ring (H-C-H, C-C, CH_2-N and CH_3-(N)-CN) [60].

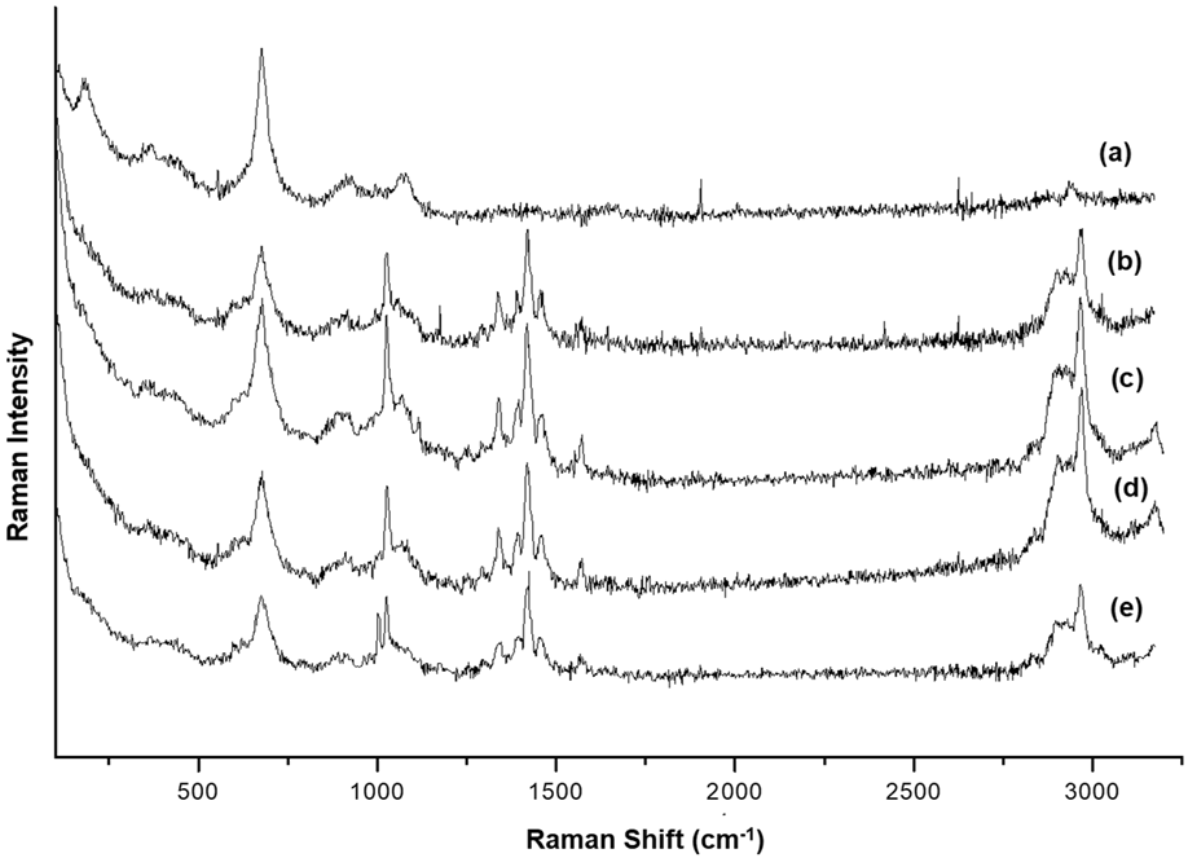

Figure 4- RAMAN spectra of samples (a) SSMMP-Ni 50%, (b) SSMMP-Ni 50%-AMO Br, (c) SSMMP-Ni 50%-AMO I, (d) SSMMP-Ni 50%-IMI Br and (e) SSMMP-Ni 50%-IMI I

XRD

Samples XRD patterns are shown in Figure 5. ST-Ni 50% (Figure 5, h) presented inter-reticular distance values (d) with reflections at 001 (9.99 Å), 020 (4.53 Å), 003 (3.17 Å) and 060-330 (1.52 Å), characteristics of Mg/Ni synthetic talc [33,61]. SSMMP-Ni 50% and SSMMP-Ni 100% (Figure 5, a and b) showed no reflection, evidencing the formation of amorphous structures of SSMMP composed by two or three Mg and/or Ni octahedrons and three or four Si tetrahedrons located at the top and the bottom of the octahedral sheet; [33,34]. For samples functionalized with ILs (SSMMP-Ni 50%-IL, Figure 5 c-g), a weak reflection at $2\theta = 6^{o}$ is observed due to an increment in sample structure organization caused by the surfactant effect of the organo-alkoxysilanes present in the synthesis process acting as an anionic surfactant [62]. Yet, hydrophilic groups form micelles facilitating Si-O-Mg covalent bond formation and assisting the lamellar structure growth [34].

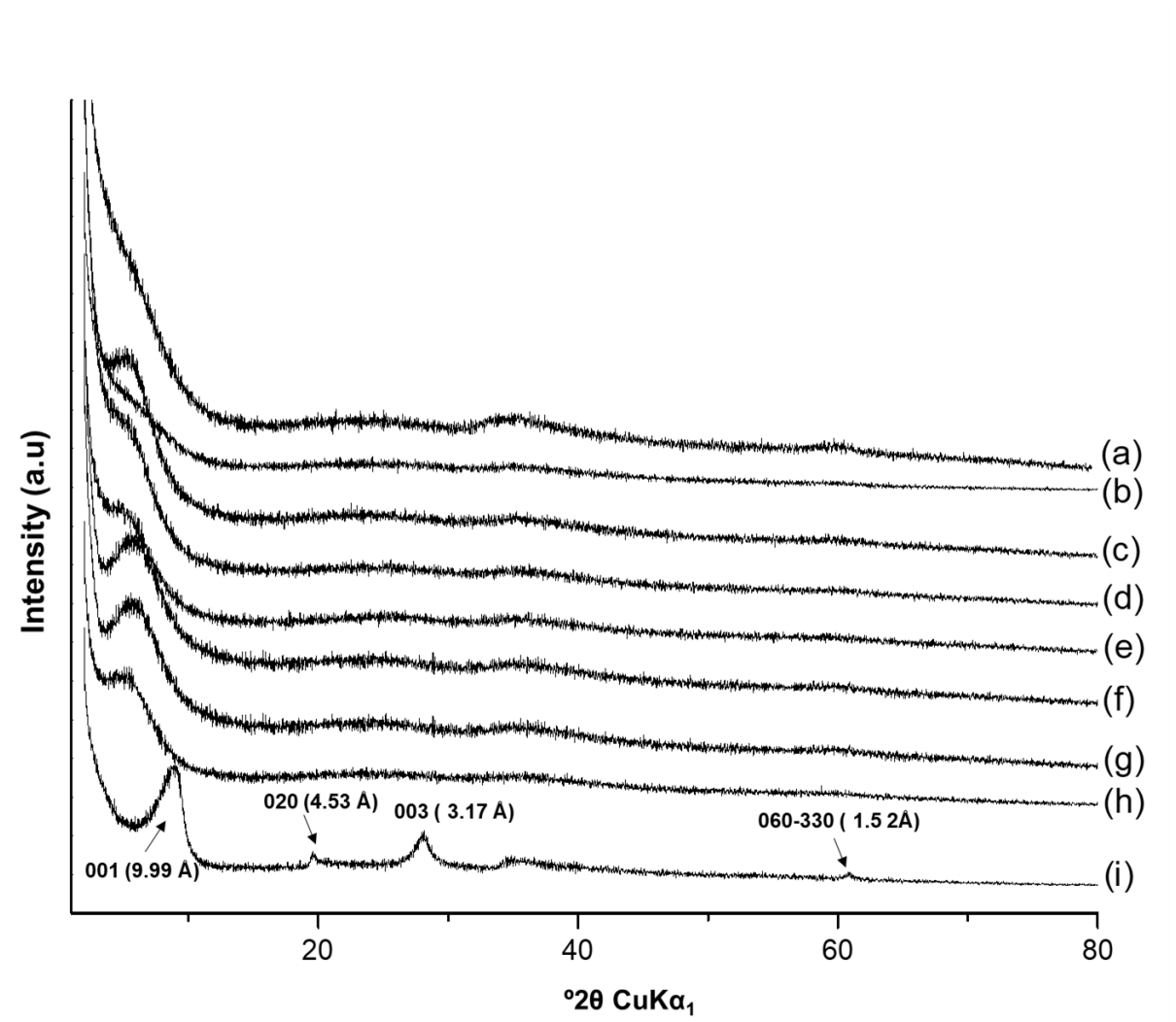

Figure 5- DRX patterns of samples (a) SSMMP-Ni 50%, (b) SSMMP-Ni 100%, (c) SSMMP-Ni 50%-AMO Cl (d) SSMMP-Ni 50%-IMI I, (e) SSMMP-Ni 50%-IMI Br, (f) SSMMP-Ni 50%-IMI Cl, (g) SSMMP-Ni 50%-AMO I, (h) SSMMP-Ni 50%-AMO Br and (i) ST-Ni 50%.

TGA

Synthesized samples were characterized by TGA as seen in Table 2. Results show that all samples have a first mass loss attributed to the loss of physisorbed water. The second mass loss refers to the loss of Si-OH, Mg-OH and Ni-OH groups present on the synthetic talc sheet edges (for ST-Ni 50%) or present in the surface of SSMMP [7,63]. For samples functionalized with IL, the second step is also related to imidazolium (starting near 280°C) and ammonium cations degradation (starting near 250°C) [53,64]. The third mass loss, appearing for synthetic talc ST-Ni 50%, refers to the dehydroxylation of talc sheets accompanied by the formation of enstatite and silica [51,63].

Table 2- Thermogravimetric analyses

Sample	1st mass loss		2nd mass loss		3rd mass loss	
	T_{onset} - T_{endset} (°C)	w/w %	T_{onset} - T_{endset} (°C)	w/w %	T_{onset} - T_{endset} (°C)	w/w %
ST-Ni 50%	25-137	4.4	137-550	2.9	550-900	3.0
SSMMP-Ni 50%	25-243	15.1	243-900	7.8	-	-
SSMMP-Ni 100%	25-258	16.2	325-900	7.4	-	-
SSMMP-Ni 50%-AMO Br	25-245	14.4	245-900	13.9	-	-
SSMMP-Ni 50%-AMO Cl	25-251	15.1	251-900	16.0	-	-
SSMMP-Ni 50%-AMO I	25-237	14.3	237-900	13.2	-	-
SSMMP-Ni 50%-IMI Br	25-293	10.8	293-900	13.2	-	-
SSMMP-Ni 50%-IMI Cl	25-283	13.5	283-900	18.0	-	-
SSMMP-Ni 50%-IMI I	25-279	11.9	279-900	12.0	-	-

BET

Table 3 presents the samples specific surface areas. SSMMP-Ni 50% and SSMMP-Ni 100% present higher specific surface area when compared to ST-Ni 50% and SSMMP functionalized with IL (see Table 3, entries 2 and 3). SSMMP-Ni 50% was submitted to hydrothermal treatment to produce synthetic talc ST-Ni 50% decreasing the material specific surface area (from 285 m^2/g to 195 m^2/g). The drop in sample specific surface area after heat treatment results from the growth of SSMMP entities forming stacked lamellae with temperature [33,51]. The decrease in the specific surface area of the IL functionalized samples (see Table 3, entries 4 to 9) indicates the success of the IL insertion in the SSMMP structure [6,7]. Somehow the synthesis method of samples functionalized with IL interferes on the specific surface area value. Samples with Cl as anion undergo no anion exchange, while I and Br are inserted in the molecule by an ionic exchange reaction having NaCl as a byproduct. NaCl remains in the next step of the synthesis, probably facilitating defect creation during the washing process increasing specific surface area [65–67]. This idea can be corroborated by N_2 sorption/desorption curves showing a decrease in the N_2 volume adsorbed by the samples containing the Cl^- anion (see Figure S1).

Table 3- Samples specific surface areas

Entry	Sample	S_{BET} (m^2/g)
1	ST-Ni 50%	145
2	SSMMP-Ni 50%	285
3	SSMMP-Ni 100%	340
4	SSMMP-Ni 50%-AMO Br	180

5	SSMMP-Ni 50%-AMO Cl	9.7
6	SSMMP-Ni 50%-AMO I	176
7	SSMMP-Ni 50%-IMI Br	211
8	SSMMP-Ni 50%-IMI Cl	27
9	SSMMP-Ni 50%-IMI I	213

329

330 *SEM*

331 Samples morphology is shown in Figure 6. ST-Ni 50% (Figure 6, a and b) has a dense
332 and compact structure, formed by numerous stacked lamellae. Samples undergoing
333 no heat treatment (SSMMP-Ni 50%, 100% and SSMMP-Ni 50%-IL) (Table 3, entries
334 2-9) showed agglomerated spherical morphology as seen in Figure 6 (c) and (d)
335 (samples SSMMP-Ni 50% and SSMMP-Ni 50%-AMO Br, respectively). CO_2 sorption
336 capacity is influenced by sample morphology. A particulate morphological structure
337 fosters CO_2 adsorption as seen in the next section.

338

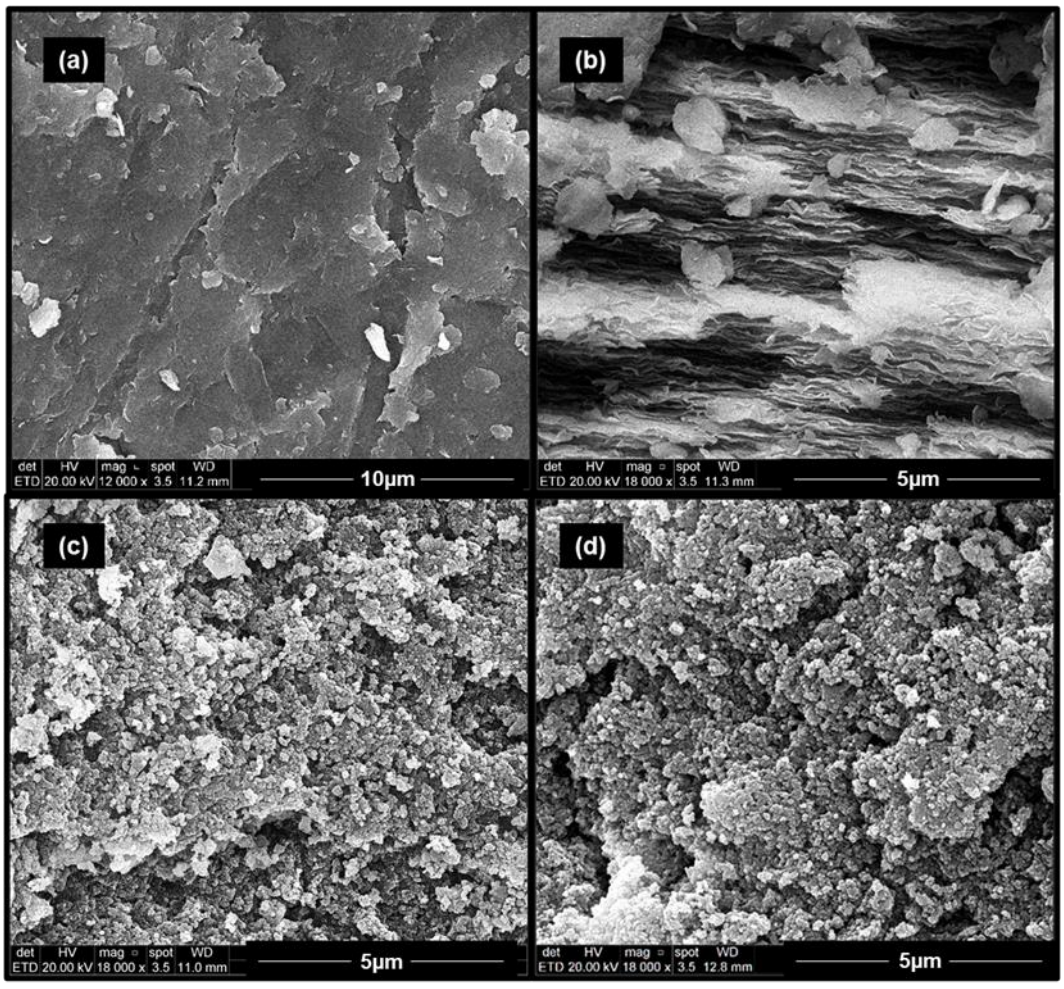

339

340 Figure 6- Samples SEM images: (a) and (b) ST-Ni 50%, (c) SSMMP-Ni 50% and (d)
341 SSMMP-Ni 50%-AMO Br

3.1 CO_2 sorption tests

CO_2 sorption tests at CO_2 equilibrium pressures of 1 bar, 10 bar, and 30 bar of CO_2 at 25°C are shown in Table 4. As expected, the synthetic talc ST-Ni 50% (Table 4, entry 1) showed the lowest CO_2 sorption capacity among the analyzed samples. The low CO_2 sorption capacity presented by ST-Ni 50% is directly related to its lamellar structure composed of an octahedral sheet of Mg and Ni sandwiched by two tetrahedral sheets of Si presenting reactive groups (-SiOH and -MOH where M = Mg and Ni) only on the edges of these sheets (representing only 10% of the total surface) [34,35]. According to previously published work [7], the OH groups are essential for the CO_2/adsorbent interaction. The CO_2 sorption in adsorbents rich in Si-OH groups occurs by physical adsorption through dispersive and electrostatic interactions, by weak interaction of CO_2 with the OH group present on the surface of these materials ($H^{\delta+} \cdots {}^{\delta-}O=C=O^{\delta-}$) [7,68]. The above statement can be corroborated by comparing the CO_2 sorption capacity of synthetic talc ST-Ni 50%, and its precursor SSMMP-Ni 50% (undergoing no thermal treatment) and SSMMP-Ni 100% (100% of the Mg replaced by Ni, undergoing no thermal treatment) (Table 4, entries 2 and 3, respectively). Comparing these two precursors with ST-Ni 50%, an increase of 0.61 $mmolCO_2/g$ and 0.48 $mmolCO_2/g$ in the CO_2 sorption capacity, respectively, is observed at 1 bar. Unlike synthetic talc, SSMMP-Ni X% are formed by a few Si tetrahedra bonded together, sandwiching 1-3 octahedra of Mg/Ni (as shown in Figure 7), this configuration allows the presence of greater amounts of reactive groups (-SiOH and -MOH where M= Mg and Ni) on the SSMMP surface and consequently higher interaction with the CO_2 [7,33,34,51].

Table 4 – Samples sorption capacity at 25ºC in different CO_2 equilibrium pressures

Entry	samples	CO_2 sorption		
		1 $bar_{eq.}$ ($mmolCO_2/g$)	**10 $bar_{eq.}$ ($mmolCO_2/g$)**	**30 $bar_{eq.}$ ($mmolCO_2/g$)**
1	ST-Ni 50%	0.97 (±0.06)	2.42 (±0.09)	4.05 (±0.23)
2	SSMMP-Ni 50%	1.58 (±0.07)	3.26 (±0.18)	5.49 (±0.19)
3	SSMMP-Ni 100%	1.45 (±0.06)	4.21 (±0.20)	6.15 (±0.18)
4	SSMMP-Ni 50%-AMO Br	1.91 (±0.06)	3.84 (±0.16)	8.22 (±0.27)
5	SSMMP-Ni 50%-AMO Cl	1.25 (±0.06)	3.07 (±0.11)	4.63 (±0.06)

6	SSMMP-Ni 50%-AMO I	1.73 (±0.07)	3.65 (±0.04)	5.66 (±0.13)
7	SSMMP-Ni 50%-IMI Br	1.64 (±0.05)	3.42 (±0.06)	7.92 (±0.15)
8	SSMMP-Ni 50%-IMI Cl	1.18 (±0.05)	2.87 (±0.12)	4.45 (±0.23)
9	SSMMP-Ni 50%-IMI I	1.61 (±0.05)	3.73 (±0.08)	4.98 (±0.13)

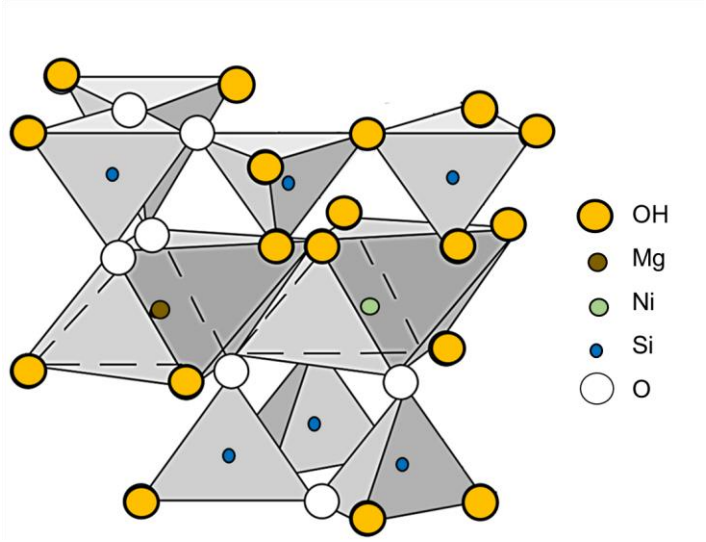

Figure 7- SSMMP-Ni 50% structure

At low CO_2 equilibrium pressures, the SSMMP-Ni 50% functionalized with the ILs AMO-Br, AMO-I, IMI-Br and IMI-I (Table 4, entries 4,6,7 and 9, respectively), demonstrated slightly higher CO_2 sorption capacity when compared to pristine SSMMP-Ni 50% (Table 4, entry 2). Even with the decrease in the specific surface area, the SSMMP containing the ILs demonstrated a good CO_2 sorption capacity evidencing the affinity CO_2/IL. By analyzing the behavior of ammonium (AMO+) and imidazolium (IMI+) cations in CO_2 capture, it can be seen that, regardless of the anion, SSMMP-containing ammonium cation presented superior CO_2 sorption capacity. The same behavior was observed by Tang et al., (2009) [69] when studying the CO_2 sorption capacity in different poly (ionic liquids) containing ammonium and imidazolium cations. This behavior was attributed to a stronger interaction between the ammonium cation and CO_2 compared to the imidazolium cation and CO_2. Ammonium cation possesses a strong positive charge density compared to the delocalized positive charge of the imidazolium cation facilitating CO_2/IL interaction [70].

Furthermore, from the results shown in Table 4, it can be observed that the anion also plays an important role in CO_2 sorption. When comparing the anions Br^- and I^-, it is observed that regardless of the cation, the anion Br^- has better CO_2 sorption capacity when compared to the anion I^-. For halide anions, the interaction strength (binding energy) between anion-CO_2 decreases with increasing anion size, explaining the Br^- superior sorption capacity [71]. Zhou et al.,(2016) [73] synthesized ZrP and MMT nano-sheets grafted with the IL BMIM Cl and analyzed their CO_2 sorption capacity. According to the author, at temperatures close to 40ºC and at low CO_2 pressures, CO_2 sorption occurs by physical adsorption. Pristine SSPPM-Ni 50% and SSPPM-Ni 50% IL also adsorbs CO_2 by physisorption through the reactive groups (-SiOH and -MOH where M = Mg and Ni) of the SSMMP-Ni 50% surface and the ILs. In a recently published work by the group [7] two imidazolium-based ILs were functionalized onto Mg-based SSMMP varying the amount of silica substituted by grafted ILs from 5% to 20%. In conclusion, there is an ideal amount of IL to be functionalized on the SSMMP to maintain the synergistic relation between IL/reactive groups on the surface of the SSMMP.

3.2 CO_2/ N_2 selectivity tests

Figure 8 presents CO_2 selectivity in CO_2/N_2 mixtures for samples SSMMP-Ni X% and SSMMP-Ni 50%-IL. Comparing SSMMP-Ni X% with IL functionalized samples, it is clear that IL plays a role in CO_2 selectivity as previously related in literature [7,26,29,72,74]. The functionalization of SSMMP-Ni 50% with IMI-Br and AMO-Br increased CO_2 selectivity from 6.5 (±0.29) to 14.4 (±0.35) and 13.1 (±0.47), an increase of 121.5% and 101.5% in CO_2 selectivity, respectively. So the cation plays a role in CO_2 selectivity: SSMMP-Ni 50%-IMI samples are more selective for CO_2 when compared to SSMMP-Ni 50%-AMO with the same anion (see Figure 8). The anion also plays a role in CO_2 selectivity, Br^- being the most selective above I^- and Cl^- (see Figure 8).

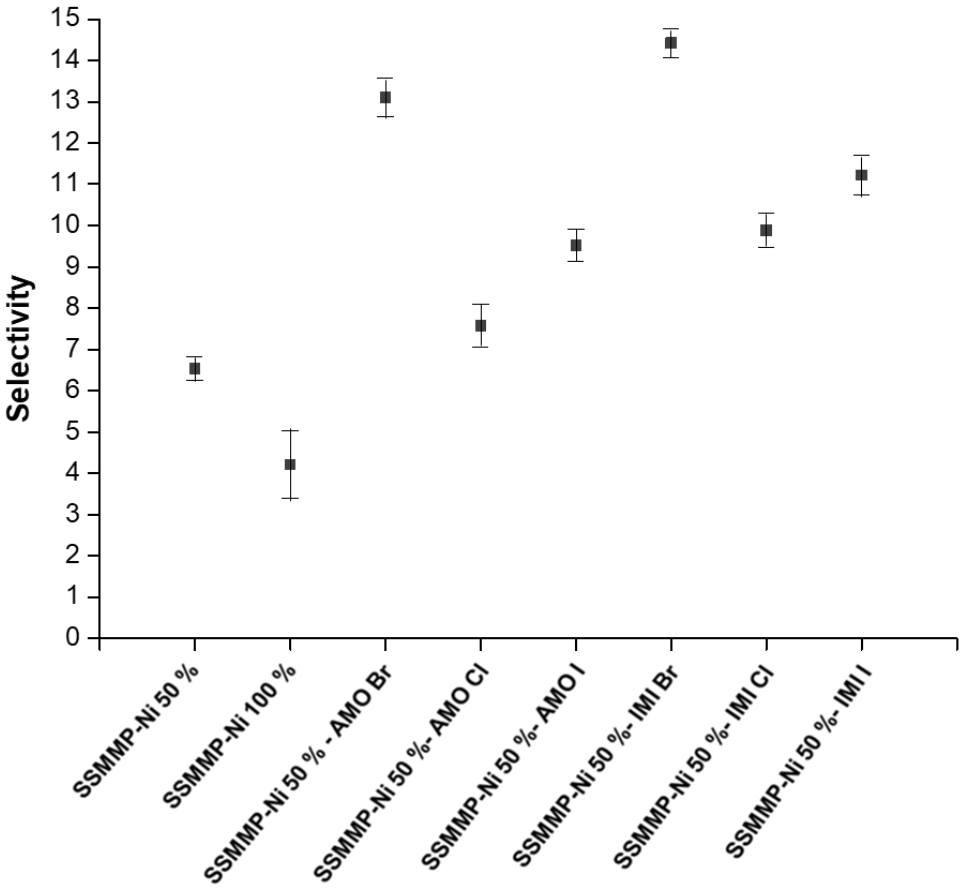

Figure 8 – CO_2 selectivity in CO_2/N_2 mixtures at 25°C and mixture equilibrium pressure of 20 bar.

Table 5 presents sorption capacity and CO_2 selective sorption for ionic liquids functionalized silica-based materials reported in the literature. As seen in Table 5, the SSMMP-Ni 50%-IL presented higher CO_2 sorption capacity at 1 bar when compared to the different sorbents represented in Table 5. Yet, when comparing the synthesis methods of most silica-based supports (Table 5) with SSMMP-Ni 50%-IL, the advantages of the sorbents described in this work are obvious even more when one considers that there is no need for organic solvents or thermal treatment for their synthesis. SSMMP are thus low-cost and energy expenditure sorbent materials.

Table 5- CO_2 sorption values for different inorganic silicate materials found in the literature

Sample	Analyses conditions	Sorption (mmol CO_2/g)	N_2/CO_2 selectivity	Ref.
Si-[P_{8883}]TFSI/SiO_2	1 bar,40ºC	0.99	~6.0	[75]
SIL-15% - [C_4 TPIm] [Cl]	4 bar,45ºC	1.45	2.7	[26]

SIL-15% - [i-C 5 TPIm] [Cl]	4 bar,45ºC	1.50	4.5	[26]
SiO_2 –Si – P_{4443} BF_4	1 bar,25ºC	~0.60	8	[76]
SiO_2 –Si – P_{8883} BF_4	1 bar,25ºC	~0.61	6	[76]
MCMRH-IL-A20	4 bar,25ºC	1.25	-	[53]
MCMRH-IL-B10	4 bar,25ºC	1.77	-	[53]
SSMMP-5%-Im(nBu)-I	1 bar,25ºC	0.89	16.9	[7]
SMMP-5%-Im(nBu)-NTf_2	1 bar,25ºC	0.95	-	[7]
S-mBmim [Tf_2N]-10	4 bar,45ºC	~1.27	3.7	[77]
S-mBmim [Br]-10	4 bar,45ºC	~1.67	4.8	[77]
ILClM50	1 bar,25ºC	0.75	-	[78]
MCM-41/[VBTMA][Cl]	1 bar,40ºC	0.64	-	[29]
SIL-AAB-IL	1 bar,25ºC	1.04	-	[79]
SIL-IB-IL	1 bar,25ºC	0.61	-	[80]
MMT-BMIMCl-1-2.0	1 bar,30ºC	0.40	-	[72]
SSMMP-Ni 50%-AMO Br	1 bar,25ºC	1.91	13.1	This work
SSMMP-Ni 50%-IMI Br	1 bar,25ºC	1.64	14.4	This work

3.3 Sorbents structural stability

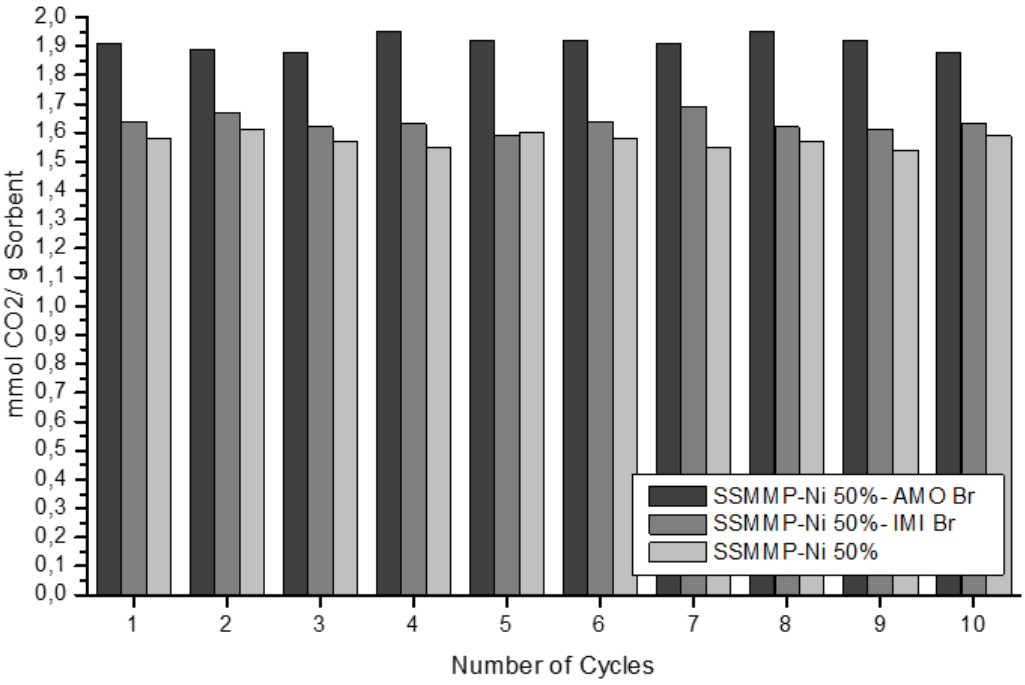

Figure 9- Sorption/desorption CO_2 tests performed at 1 bar CO_2 pressure and 25ºC.

Figure 9 presents the cyclability tests of CO_2 sorption/desorption for SSMMP-Ni 50%-AMO Br, SSMMP-Ni 50%-IMI-Br and SSMMP-Ni 50%. CO_2 sorption capacity was constant after 10 cycles of CO_2 sorption/desorption. FTIR analysis was performed on samples before and after the 10 cycles and no structural changes were observed. See supplementary material (S2).

3.4 CO_2 cycloaddition in epoxide

Table 5 presents the results for solvent-free cyclic carbonate syntheses using SSMMP-Ni X% and SSMMP-Ni 50%-IL as heterogeneous catalysts. Tests carried out with SSMMP-Ni 50% and SSMMP-Ni 50%-IL (Table 6, entries 3-9), with no cocatalyst addition (TBAB) presented a low propylene carbonate conversion. SSMMP-Ni 50%-IL low catalytic activity is probably due to the interaction between the IL and the acidic hydroxyl groups on the catalyst surface preventing the nucleophilic attack of the halide anion to the less hindered carbon of the epoxide molecule, at the same time as preventing CO_2 interaction with -SiOH, -MgOH and -NiOH groups [72,81,82]. Yet, SSMMP-Ni 50%-IMI Br, SSMMP-Ni 50%-IMI I, SSMMP-Ni 50%- AMO Br and SSMMP-Ni 50%- AMO I present a strong CO_2/IL interaction (as seen in section 3.1), difficulting the IL/epoxide interaction, the epoxide ring opening and the subsequent CO_2 insertion into the epoxide ring and cyclic carbonate formation [27]. For ST-Ni 50% and SSMMP-Ni 50% (Table 6, entries 2 and 3), low catalytic activity was expected due to the lack of a nucleophilic agent in the catalyst [82]. The addition of TBAB as cocatalyst in the reactions with ST-Ni 50%, SSMMP-Ni 50% and SSMMP-Ni 100% (Table 6, entries 10, 12-19), increased the catalytic activity. When comparing the catalytic performance of SSMMP-Ni 50% and ST-Ni 50% (Table 6), a drop of 24.5% in the propylene carbonate yield is observed. The low catalytic activity of ST-Ni 50% is attributed to the lower number of OH groups in the catalyst surface, due to heat treatment, allied to the difficulty of CO_2 interaction with the Lewis acid sites (Mg and Ni) of the octahedral layer of the lamellar structure of synthetic talc. Comparing samples containing 0%, 50% and 100% of Ni replacing Mg in the octahedral structure (Table 6, entries 11, 12 and 18, respectively), an increase of 31.2 % in carbonate yield was observed when 50% of Mg was replaced by Ni. When 100% of Mg was replaced by Ni no significant increase in propylene carbonate yield was observed. Aiming to evaluate the possibility of using the same material as sorbent/catalyst, a cycloaddition reaction using SSMMP-50%-R (Table 6, entry 16) previously used in the CO_2 sorption, CO_2/N_2 separation, and

submitted to 10 CO_2 sorption/desorption cycles was tested as catalyst. When comparing the result of bare SSMMP-Ni 50% with reused SSMMP-Ni 50%-R, a similar propylene carbonate yield was obtained. This result reveals the possibility of reusing SSMMP-Ni X% as heterogeneous catalysts after they are used as solid sorbent in CO_2 capture. Structural analysis of the SSMMP-Ni 50%-R was performed before and after it was used as a catalyst showing no changes as seen in Figure S2.

Table 6- Catalytic performance of synthesized materials in the cyclic propylene carbonate syntheses.

Entry	Sample	Cocat.	Conversion (%)	Selectivity (%)	Yield (%)
1	TBAB[a]	-----	35.6	97.1	35
2	ST-Ni 50%[a]	-----	9.8	-	-
3	SSMMP-Ni 50%[a]	-----	9.3	-	-
4	SSMMP-Ni 50%-AMO Br[a]	-----	5.5	-	-
5	SSMMP-Ni 50%-AMO Cl[a]	-----	3.7	-	-
6	SSMMP-Ni 50%-AMO I[a]	-----	2.9	-	-
7	SSMMP-Ni 50%-IMI Br[a]	-----	6.7	-	-
8	SSMMP-Ni 50%-IMI Cl[a]	-----	13.5	-	-
9	SSMMP-Ni 50%-IMI I[a]	-----	7.2	-	-
10	ST-Ni 50%[a]	TBAB	72.6	90.9	65.7
11	SSMMP(0%Ni)[a]	TBAB	60.0	98.4	59.0
12	SSMMP-Ni 50%[a]	TBAB	91.8	98.3	90.4
13	SSMMP-Ni 50%[b]	TBAB	86.2	94.3	81.2
14	SSMMP-Ni 50%[c]	TBAB	94.2	99.0	93.3
15	SSMMP-Ni 50%[d]	TBAB	88.8	98.3	87.3
16	SSMMP-Ni 50%-R* [e]	TBAB	93.6	96.1	89.9
17	SSMMP-Ni 50%[f]	TBAB	86.5	98.7	85.3
18	SSMMP-Ni 100%[a]	TBAB	96.6	93.2	90.0
19	SSMMP-Ni 100%[d]	TBAB	91.1	95.2	86.7

Reactional conditions: [a]20 bar, 100ºC and 7h; [b]20bar, 90ºC and 7h; [c]20 bar, 110ºC and 7h; [d]15 bar, 100ºC and 7h;[e]SSMMP-Ni 50% after 10 sorption/desorption CO_2 cycles; [f]20 bar, 90ºC and 5h; 0.1 mol EP,TBAB 0.6 mol% of PE and 0.2 g of catalyst.

SSMMP-Ni 50% stability and reaction conditions effect (pressure, temperature and reaction time) on the catalytic performance in propylene carbonate synthesis was evaluated (Figure 10, (a), (b) and (c). CO_2 pressure variation (10-30 bar) was performed at 100ºC and 7 hours of reaction time. As seen in Figure 10 (a), when increasing the CO_2 pressure from 10 to 25 bar, a subtle increase in the propylene carbonate yield is observed, from 86.2% to 92.0%. However, when increasing CO_2 pressure to 30 bar, the cyclic carbonate yield drops from 92.0% to 86.1%, indicating

that at higher CO_2 pressures the catalytic activity of SSMMP-Ni 50% decreases. The effect of temperature was evaluated by maintaining 20 bar of CO_2 pressure and a reaction time of 7 hours and varying the reaction temperature from 60°C to 110°C. The temperature elevation increased the cyclic propylene carbonate yield from 44.8% to 93.3%, respectively proving the influence of temperature on the catalytic activity of SSMMP-Ni 50%. The variation of the reaction time (2-7 h) was carried out keeping the temperature of 100ºC and 20 bar of CO_2 pressure. Increasing reaction time from 2 h to 4 h increases catalytic activity and propylene carbonate yield from 59.4% to 85.9%, respectively. After 4 hours of reaction time, the carbonate yield becomes stable, showing a slight increase until reaching a yield of 90.4% after 7 hours. Based on the results described above, a synthesis under reaction conditions of 20 bar, 90°C and 5 hours was carried out (Table 6, entry 17) and a yield of 85.3% of propylene carbonate was obtained, showing that reaction conditions of 20 bar, 100ºC and 7 hours as ideal.

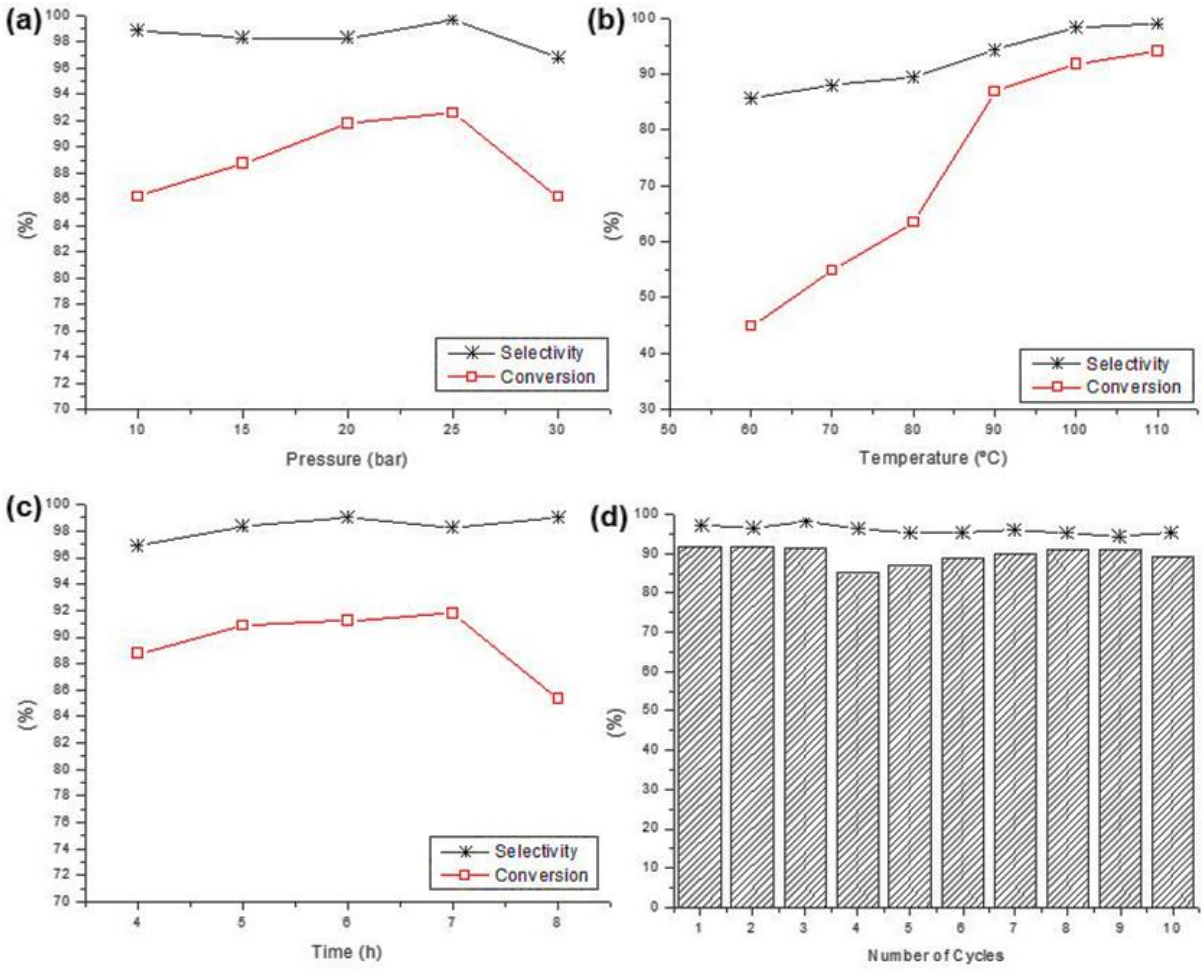

Figure 10- Evaluation of reactional condition variation effect in cyclic propylene carbonate syntheses and cycles of sorption/desorption using SSMMP-Ni 50%: effect of (a) pressure, (b) temperature, (c) reaction time and (d) number of cycles.

The stability of SSMMP-Ni 50% used as catalyst was investigated using the same sample for 10 consecutive reaction cycles, under reaction conditions of 20 bar, 100 ºC and 7h. As seen in Figure 10 (d), conversion and selectivity are constant indicating the high stability of the SSMMP-Ni 50% as catalyst in cycloaddition reaction. A structural investigation of the catalyst was performed by infrared spectroscopy before and after the 10 cycles and the spectrograms are shown in Figure S3. The catalyst structure is unaltered, being visible cocatalyst residue remaining after water washing.

The catalytic performance of SSMMP-Ni 50% in the cycloaddition reaction using 3 new substrates was investigated (Table 7). The reactions were carried out using TBAB as cocatalyst (0.6 mol% of the substrate), at 20 bar of CO_2 pressure, at 100ºC of temperature, for 7h. SSMMP-Ni 50% presents a good catalytic performance for all cyclic carbonate syntheses, as seen in Table 7. This behavior differs from some results described in the literature, reporting the drop in the cyclic carbonate yield with the increase of the side chain linked to the epoxide ring. This behavior is attributed to the hysterical hindering caused by the molecule size making it difficult the interaction of the catalyst active sites with the epoxide molecule [82]. Among the tested substrates, the highest yield was found for 1,2-butylene carbonate (85.2%) and the lowest for chloropropene carbonate (92.9%) due to the low selectivity of the reaction.

Table 7- Catalytic performance of SSMMP-Ni 50% in addition cycle reactions with different epoxides

Reagent	Product	Selectivity	Yield (%)
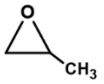	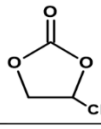	98.3	90.4
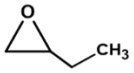	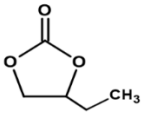	87.1	85.2
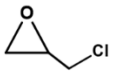	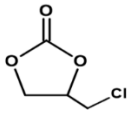	99.9	92.9
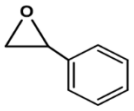	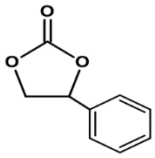	99.9	90.1

521

522 Table 8 presents, for comparison, results from the literature on the catalytic
523 performance of natural phyllosilicates and layered double hydroxide (LDH). When
524 comparing the synthesis (or preparation) steps of materials described in the literature
525 to this work, it can be highlighted that, unlike the other catalysts, in the SSMMP-Ni 50%
526 synthesis no organic solvents are needed for material exfoliation nor calcination at high
527 temperatures since SSMMP is obtained prior to the formation of the organized and
528 lamellar structure of synthetic talc, before the hydrothermal treatment. At this stage,
529 SSMMP-Ni X% have reactive groups (Si-OH, Ni-OH, and Mg-OH) distributed across
530 their surface. These groups make it easier for the material to interact with CO_2,
531 epoxide, and other reagents, and also facilitate their functionalization. Regarding
532 reaction conditions, the use of moderate reaction conditions without the need for
533 organic solvents during the addition cycle reactions for SSMMP should be highlighted.
534 The high and easy reuse of SSMMP-Ni 50%, with no drop in conversion and selectivity,
535 is another indicator of the good potential of these materials as heterogeneous
536 catalysts.

537 Table 8- Comparing the catalytic behavior of different materials

Catalyst	Cocatalyst / Solvent	Reaction conditions	Yield (%)	Ref.
Talc[(a)]	TBAB / CH_3CN	140ºC, 30 bar, 20h	92.7	[83]
Biotite[(a)]	TBAB / CH_3CN	120ºC, 20 bar, 20h	30.4	[83]
Chlorite[(a)]	TBAB/ CH_3CN	120ºC, 20 bar, 20h	38.7	[83]
Phlogopite[(a)]	TBAB / CH_3CN	120ºC, 20 bar, 20h	35.0	[83]
Vermiculite[(a)]	TBAB / CH_3CN	150ºC, 30 bar, 20h	86.8	[83]

slagLDH(600)[(b)]	- / DMF	100ºC, 1 bar, 48h	90.0	[84]
MgFeAl-LDH (WE)[(c)]	TBAB / -	50ºC, 5 bar, 7h	96.2	[82]
Montmorillonite[(b)]	TBAB / -	100ºC, 1 bar, 24h	--	[85]
slagHC(Cl)(800)[(b)]	- / DMF	100ºC, 1 bar, 24h	85	[86]
Smectite-Mg-Na-K-4[(a)]	- / -	150ºC, 80 bar, 15h	80.7	[87]
SSMMP-Ni 50%[(a)]	TBAB / -	100ºC, 20 bar, 7h	90.4	This work

[(a)] Propylene epoxide; [(b)] Styrene epoxide; [(c)] Epichlorohydrin.

3.1 Proposed catalytic mechanism

Figure 11 presents a catalytic mechanism proposition based on previously described works in the literature [81,82]. The main catalytic route involves metal ions (Mg and Ni) acting as Lewis's acid activators attracting the epoxide ring oxygen to bind to them. The bromide anion (Br^-) of the nucleophile TBAB attacks the least hindered carbon of the epoxide ring (1) to form the oxyanion intermediate (2). Simultaneously, the electron-rich oxygen atom of the groups (-MgOH and -SiOH) reacts with CO_2 leading to the formation of the carbonate anion, after the O- of the carbonate anion attacks the bromine-anchored carbon atom (3) dissociating the C-Br bond (4). Finally, the corresponding cyclic carbonate can be produced by closing the intramolecular ring (5), and the catalyst is regenerated to the next epoxide molecule (6). A second catalytic cycle is probably occurring simultaneously, but less probable to be occurring due to the competition of epoxide and CO_2 for the interaction with metal ions. The proposed catalytic route starts with CO_2 adsorbed by the Lewis acid metal ions (Mg and Ni) of the SSMMP-Ni 50% (3*), resulting in the intermolecular nucleophilic addition of the oxy-anion intermediate to form a metal carbonate intermediate (4*). Then next, intramolecular ring closure of the carbonate anion intermediate (5), yields the corresponding cyclic carbonate as in cycle 1, and catalyst regeneration occurs.

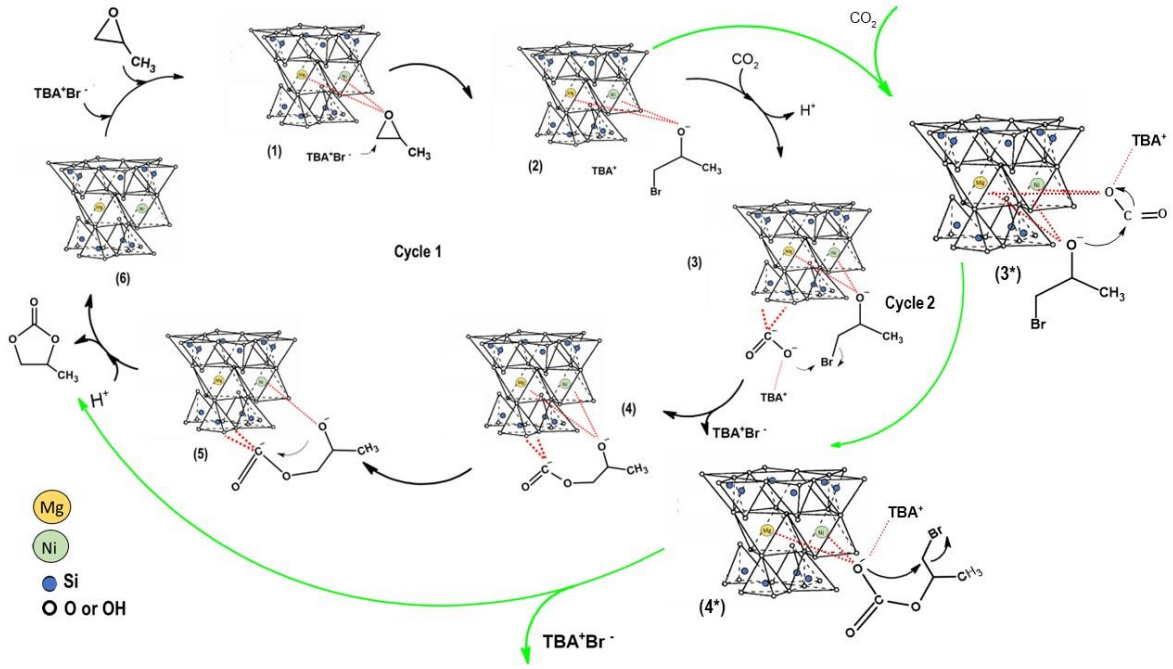

Figure 11- Proposal of the catalytic route for the synthesis of cyclic carbonates using SSMMP-X% as a catalyst

4. Conclusion

In this work, we report the synthesis, characterization and use of synthetic silico-metallic mineral particles (SSMMP-Ni) and SSMMP-Ni functionnalized with IL. These materials proved to be highly efficient stable (1) solid adsorbents in CO_2 capture from CO_2/N_2 gas mixtures, (2) heterogeneous catalysts in the solvent-free cyclic carbonates synthesis, with easy catalyst/product separation. SSMMP-Ni 50%-AMO Br showed the best performance of CO_2 sorption, reaching 1.91 mmol of CO_2/g at 1 bar and 8.22 mmol of CO_2/g at 30 bar. For CO_2/N_2 separation, SSMMP-Ni 50%-IMI Br showed the highest selective capacity (14.4). It was evidenced that both the IL anion and cation influence the sorption capacity and selectivity. The ammonium cation is more efficient in capturing CO_2 and imidazolium is more selective for capturing CO_2 in CO_2/N_2 mixture. Among the anions, Br^- presents the highest interaction energy with CO_2, presenting better performance both for pure CO_2 sorption and CO_2 selectivity. In catalysis, the sample containing 50% of Ni replacing Mg, presented the best catalytic performance, reaching conversion and selectivity in propylene carbonate production superior to 90%. It was also evidenced the possibility of reusing the SSMMP-Ni 50%-R sample as a catalyst in the synthesis of cyclic carbonates, after was used in 10 cycles of CO_2 sorption/desorption, evidencing the possibility of this material being used in CO_2 capture and transformation. The easy synthesis of these materials (one-pot), using low-cost reagents, without the use of organic solvents and with low energy expenditure, allied to the good results presented in this work, point to the potential of the use of SSMMP in the industry both in CO_2 capture in post-combustion process, as well as in chemical transformation after its capture.

Acknowledgment

This study was written by some members of the Capes- PRINT Internationalization Project from PUCRS University and was financed in part by the Coordination for the Improvement of Higher Education Personnel- Brasil (CAPES) – Finance Code 001. Sandra Einloft thanks CNPq for the research scholarship.

592 **Bibliography**

593 [1] O. Tursunov,, L. Kustov,, A. Kustov, Oigyl & Gas Science and Technology
594 72(2017) (2019) 1–9. 10.2516/ogst/2017027.

595 [2] I.H. Arellano,, S.H. Madani,, J. Huang,, P. Pendleton, Chemical
596 Engineering Journal 283 (2016) 692–702. 10.1016/j.cej.2015.08.006.

597 [3] B. Ozcan,, E. Gultekin, Eurasian Journal of Business and Economics 9(18)
598 (2016) 113–34. 10.17015/ejbe.2016.018.07.

599 [4] M.T. Ravanchi,, S. Sahebdelfar, Process Safety and Environmental
600 Protection 145 (2021) 172–94. 10.1016/j.psep.2020.08.003.

601 [5] R.M. Cuéllar-Franca,, A. Azapagic, Journal of CO2 Utilization 9 (2015) 82–
602 102. 10.1016/j.jcou.2014.12.001.

603 [6] M. Younas,, M. Rezakazemi,, M. Daud,, M.B. Wazir,, S. Ahmad,, N. Ullah,,
604 Inamuddin,, S. Ramakrishna, Progress in Energy and Combustion Science
605 80 (2020). 10.1016/j.pecs.2020.100849.

606 [7] D. Rodrigues,, F. Bernard,, C. Le,, E. Duarte,, P. Micoud,, A. Castillo,, F.
607 Martin,, S. Einloft, Applied Clay Science 226(May) (2022) 106572.
608 10.1016/j.clay.2022.106572.

609 [8] B. Li,, Y. Duan,, D. Luebke,, B. Morreale, Applied Energy 102 (2013) 1439–
610 47. 10.1016/j.apenergy.2012.09.009.

611 [9] J. Wang,, D. Kong,, J. Chen,, F. Cai,, L. He, Journal of Molecular Catalysis
612 A: Chemical 249 (2006) 143–8. 10.1016/j.molcata.2006.01.008.

613 [10] D. Rodrigues,, L.G. Hunter,, F.L. Bernard,, M.F. Rojas,, F. Dalla Vecchia,,
614 S. Einloft, Catalysis Letters 149(3) (2019) 733–43. 10.1007/s10562-018-

2637-4.

[11] J. Ma,, J. Liu,, Z. Zhang,, B. Han, Green Chemistry 14(9) (2012) 2410–20. 10.1039/c2gc35711a.

[12] B.M. Bhanage,, S.I. Fujita,, Y. Ikushima,, K. Torii,, M. Arai, Green Chemistry 5(1) (2003) 71–5. 10.1039/b207750g.

[13] K. Yamaguchi,, K. Ebitani,, T. Yoshida, Journal American Chemical Society 121 (1999) 4526–7. 10.1021/ja9902165.

[14] M.F. Rojas,, F.L. Bernard,, A. Aquino,, J. Borges,, F.D. Vecchia,, S. Menezes,, R. Ligabue,, S. Einloft, Journal of Molecular Catalysis A: Chemical 392 (2014) 83–8. 10.1016/j.molcata.2014.05.007.

[15] T. Yano,, H. Matsui,, T. Koike,, H. Ishiguro,, H. Fujihara,, M. Yoshihara,, T. Maeshima, Chemical Communications 2(12) (1997) 1129–30. 10.1039/a608102i.

[16] J.L. Jiang,, R. Hua, Synthetic Communications 7911(36) (2006) 3141–3148. 10.1080/00397910600908744.

[17] J. Wang,, J. Wu,, N. Tang, Inorganic Chemistry Communications 10(12) (2007) 1493–5. 10.1016/j.inoche.2007.09.022.

[18] C. Martín,, G. Fiorani,, A.W. Kleij, ACS Catalysis 5(2) (2015) 1353–70. 10.1021/cs5018997.

[19] Y. Sun,, H. Huang,, H. Vardhan,, B. Aguila,, C. Zhong,, J.A. Perman,, A.M. Al-Enizi,, A. Nafady,, S. Ma, ACS Applied Materials and Interfaces 10(32) (2018) 27124–30. 10.1021/acsami.8b08914.

[20] F. Nocito,, A. Dibenedetto, Current Opinion in Green and Sustainable

638 Chemistry 21 (2020) 34–43. 10.1016/j.cogsc.2019.10.002.

639 [21] N. Aini,, M. Razali,, K.T. Lee,, S. Bhatia,, A. Rahman, Renewable and
640 Sustainable Energy Reviews 16(7) (2012) 4951–64.
641 10.1016/j.rser.2012.04.012.

642 [22] A. Hafiidz,, M. Fauzi,, N. Aishah,, S. Amin, Renewable and Sustainable
643 Energy Reviews 16(8) (2012) 5770–86. 10.1016/j.rser.2012.06.022.

644 [23] W. Cheng,, Q. Su,, J. Wang,, J. Sun,, F.T.T. Ng, Catalysts 3(4) (2013) 878–
645 901. 10.3390/catal3040878.

646 [24] F.L. Bernard,, D.M. Rodrigues,, B.B. Polesso,, A.J. Donato,, M. Seferin,, V.
647 V. Chaban,, F.D. Vecchia,, S. Einloft, Fuel Processing Technology 149
648 (2016) 131–8. 10.1016/j.fuproc.2016.04.014.

649 [25] B. Monteiro,, R. Nabais,, A.A. Paz,, L. Cabrita,, L.C. Branco,, I.M.
650 Marrucho,, L.A. Neves,, C.L. Pereira, Energy Tech (2017) 2158–62.
651 10.1002/ente.201700228.

652 [26] R. Duczinski,, B.B. Polesso,, F.L. Bernard,, H.Z. Ferrari,, P.L. Almeida,,
653 M.C. Corvo,, E.J. Cabrita,, S. Menezes,, S. Einloft, Journal of
654 Environmental Chemical Engineering 8(3) (2020) 103740.
655 10.1016/j.jece.2020.103740.

656 [27] D.M. Rodrigues,, L.M. dos Santos,, F.L. Bernard,, I.S. Pinto,, R. Zampiva,,
657 G. Kaufmann,, S. Einloft, SN Applied Sciences 2(12) (2020) 1–11.
658 10.1007/s42452-020-03712-z.

659 [28] S. Udayakumar,, M.K. Lee,, H.L. Shim,, S.W. Park,, D.W. Park, Catalysis
660 Communications 10(5) (2009) 659–64. 10.1016/j.catcom.2008.11.017.

[29] F. Nkinahamira,, T. Su,, Y. Xie,, G. Ma,, H. Wang,, J. Li, 326 (2017) 831–8. 10.1016/j.cej.2017.05.173.

[30] J. Sun,, W. Cheng,, W. Fan,, Y. Wang,, Z. Meng,, S. Zhang, Catalysis Today 148(3–4) (2009) 361–7. 10.1016/j.cattod.2009.07.070.

[31] T. Sakai,, Y. Tsutsumi,, T. Ema, Green Chemistry 10 (2008) 337–41. 10.1039/b718321f.

[32] A. Dindi,, D.V. Quang,, L.F. Vega,, E. Nashef,, M.R.M. Abu-Zahra, Journal of CO2 Utilization 29(November 2018) (2019) 82–102. 10.1016/j.jcou.2018.11.011.

[33] A. Dumas,, M. Mizrahi,, F. Martin,, F. Requejo, 15 (2015) 5451–5463. 10.1021/acs.cgd.5b01076.

[34] M. Claverie,, A. Dumas,, C. Carême,, M. Poirier,, C. Le Roux,, P. Micoud,, F. Martin,, C. Aymonier, Chemistry - A European Journal 24(3) (2018) 519–42. 10.1002/chem.201702763.

[35] K.E. Bremmell,, J. Addai-Mensah, Journal of Colloid and Interface Science 283(2) (2005) 385–91. 10.1016/j.jcis.2004.09.048.

[36] F. Martin,, C. Aymonier,, S. Einloft,, C. Carême,, M. Poirier,, M. Claverie,, M.A. Prado,, G. Dias,, C. Quilfen,, G. Aubert,, P. Micoud,, C. Le Roux,, S. Salvi,, A. Dumas,, S. Féry-Forgues, Journal of Geochemical Exploration 200(February) (2019) 27–36. 10.1016/j.gexplo.2019.02.002.

[37] A. Dumas,, C. Le Roux,, F. Martin,, P. Micoud, METHOD FOR PREPARING A HYDROGEL COMPRISING SILICO-METALLIC MINERAL PARTICLES AND HYDROGEL WO2013093339 A1. WO 2013093339 A1, 2013.

685 [38] A. Dumas,, F. Martin,, E. Ferrage,, P. Micoud,, C. Le Roux,, S. Petit,
686 Applied Clay Science 85(1) (2013) 8–18. 10.1016/j.clay.2013.09.006.

687 [39] F.L. Bernard,, R.B. Duczinski,, M.F. Rojas,, M.C.C. Fialho,, L.Á. Carreño,,
688 V. V. Chaban,, F.D. Vecchia,, S. Einloft, Fuel 211 (2018) 76–86.
689 10.1016/j.fuel.2017.09.057.

690 [40] M. Rojas,, L. Pacheco,, A. Martinez,, K. Pradilla,, F. Bernard,, S. Einloft,,
691 L.A. Carre, 452 (2017). 10.1016/j.fluid.2017.08.026.

692 [41] W.J. Koros,, D.R. Paul, Journal of Polymer Science: Polymer Physics
693 Edition 14(10) (1976) 1903–7. 10.1002/pol.1976.180141014.

694 [42] A. Azimi,, M. Mirzaei, Chemical Engineering Research and Design 111
695 (2016) 262–8. 10.1016/j.cherd.2016.05.005.

696 [43] M. Fernández Rojas,, L. Pacheco Miranda,, A. Martinez Ramirez,, K.
697 Pradilla Quintero,, F. Bernard,, S. Einloft,, L.A. Carreño Díaz, Fluid Phase
698 Equilibria (2017) 103–12. 10.1016/j.fluid.2017.08.026.

699 [44] M.G. Da Fonseca,, C.R. Silva,, J.S. Barone,, C. Airoldi, Journal of Materials
700 Chemistry 10(3) (2000) 789–95. 10.1039/a907804e.

701 [45] E. Bahri,, S. Dikmen,, A. Yildiz,, R. Gören,, Ö. Elitok, Turkish Journal of
702 Earth Sciences 22(4) (2013) 632–44. 10.3906/yer-1112-14.

703 [46] G. Dias,, M.A. Prado,, C. Carone,, R. Ligabue,, A. Dumas,, F. Martin,, C.
704 Le Roux,, P. Micoud,, S. Einloft, Polymer Bulletin 72(11) (2015) 2991–
705 3006. 10.1007/s00289-015-1449-6.

706 [47] P. Schroeder, CMS Workshop Lectures 11(October) (2002) 181–206.

707 [48] M.A. Prado,, G. Dias,, C. Carone,, R. Ligabue,, A. Dumas,, C. Le Roux,, P.

708 Micoud,, F. Martin,, S. Einloft, Journal of Applied Polymer Science 132(16)
709 (2015) 1–8. 10.1002/app.41854.

710 [49] G. Dias,, M. Prado,, C. Carone,, R. Ligabue,, A. Dumas,, C. Le Roux,, P.
711 Micoud,, F. Martin,, S. Einloft, Macromolecular Symposia 367(1) (2016)
712 136–42. 10.1002/masy.201500141.

713 [50] F. Martin,, P. Micoud,, P. Sabatier,, A.J. Guesde,, A.J. Guesde,, P.
714 Sabatier, Can. Mineral 37 (1999) 997–1006.

715 [51] K. Chabrol,, M. Gressier,, N. Pebere,, M.J. Menu,, F. Martin,, J.P. Bonino,,
716 C. Marichal,, J. Brendle, Journal of Materials Chemistry 20(43) (2010)
717 9695–706. 10.1039/c0jm01276a.

718 [52] S. Mor,, C.K. Manchanda,, S.K. Kansal,, K. Ravindra, Journal of Cleaner
719 Production 143 (2017) 1284–90. 10.1016/j.jclepro.2016.11.142.

720 [53] R. Duczinski,, F. Bernard,, M. Rojas,, E. Duarte,, V. Chaban,, F.D.
721 Vecchia,, S. Menezes,, S. Einloft, Journal of Natural Gas Science and
722 Engineering 54(January) (2018) 54–64. 10.1016/j.jngse.2018.03.028.

723 [54] K.A. Carrado,, L. Xu,, R. Csencsits,, J. V Muntean, American Chemical
724 Society (5) (2001) 3766–73.

725 [55] M.G. da Fonseca,, C. Airoldi, Materials Research Bulletin 36(1–2) (2001)
726 277–87. 10.1016/S0025-5408(00)00470-0.

727 [56] K. Fujii,, S. Hayashi, Applied Clay Science 29(3–4) (2005) 235–48.
728 10.1016/j.clay.2005.01.005.

729 [57] J.T. Kloprogge, Raman Spectroscopy of Clay Minerals, Vol. 8, first ed.,
730 Elsevier Ltd., 2017.

[58] J. Grondin,, J. Lass,, T. Buffeteau,, R. Holomb, Raman Spectroscopy 2010(June 2010) (2011) 733–43. 10.1002/jrs.2754.

[59] M. Klein,, H. Squire,, B. Gurkan, Physical Chemistry C 124(1) (2020) 5613−5623. 10.1021/acs.jpcc.9b08016.

[60] K. Noack,, P.S. Schulz,, N. Paape,, J. Kiefer, Physical Chemistry Chemical Physics 12 (2010) 14153–61. 10.1039/c0cp00486c.

[61] M.A. Prado,, G. Dias,, L.M. dos Santos,, R. Ligabue,, M. Poirier,, C. Le Roux,, P. Micoud,, F. Martin,, S. Einloft, SN Applied Sciences 2(6) (2020) 1–13. 10.1007/s42452-020-2852-7.

[62] C.R. Silva,, M.G. Fonseca,, J.S. Barone,, C. Airoldi, Chemistry of Materials 14(1) (2002) 175–9. 10.1021/cm010474c.

[63] A. Dumas,, F. Martin,, C. Le Roux,, P. Micoud,, S. Petit,, E. Ferrage,, J. Brendlé,, O. Grauby,, M. Greenhill-Hooper, Physics and Chemistry of Minerals 40(4) (2013) 361–73. 10.1007/s00269-013-0577-5.

[64] E. V Borodina,, F. Roessner,, S.I. Karpov,, V.F. Selemenev, NANOTECHNOLOGIES IN RUSSIA 5 (2010) 808–16. 10.1134/S1995078010110091.

[65] M.S. Sader,, M. Ferreira,, M.L. Dias, Polímeros 16(1) (2006) 12–8. 10.1590/s0104-14282006000100006.

[66] S. Park,, B. Seo,, D. Shin,, K. Kim,, W. Choi, Chemical Engineering Journal 433(P1) (2022) 134486. 10.1016/j.cej.2021.134486.

[67] R.T. Tran,, E. Naseri,, A. Kolasnikov,, X. Bai,, J. Yang, Biotechnology and Applied Biochemistry 58 (2011) 335–44. 10.1002/bab.44.

754 [68] R. Malherbe,, R. Estrella,, F. Linares, The Journal Physical Chemistry C
755 114 (41) (2010) 17773–87. https://doi.org/10.1021/jp107754g.

756 [69] J. Tang,, Y. Shen,, M. Radosz,, W. Sun, Industrial and Engineering
757 Chemistry Research 48(30) (2009) 9113–8.

758 [70] J. Tang,, W. Sun,, H. Tang,, M. Radosz,, Y. Shen, American Chemical
759 Society 38 (2005) 2037–9.

760 [71] S. Yamini Sudha,, A. Khanna, World Academy of Science, Engineering and
761 Technology 33 (2009) 539–42.

762 [72] Y. Zhou,, J. Liu,, M. Xiao,, Y. Meng,, L. Sun, (2016).
763 10.1021/acsami.5b11249.

764 [73] Y. Zhou,, J. Liu,, M. Xiao,, Y. Meng,, L. Sun, ACS Applied Materials and
765 Interfaces 8(8) (2016) 5547–55. 10.1021/acsami.5b11249.

766 [74] I. Harvey,, S.H. Madani,, J. Huang,, P. Pendleton, CHEMICAL
767 ENGINEERING JOURNAL 283 (2016) 692–702.
768 10.1016/j.cej.2015.08.006.

769 [75] J. Zhu,, B. He,, J. Huang,, C. Li,, T. Ren, Microporous and Mesoporous
770 Materials 260(July 2017) (2018) 190–200.
771 10.1016/j.micromeso.2017.10.035.

772 [76] J. Zhu,, F. Xin,, J. Huang,, X. Dong,, H. Liu, Chemical Engineering Journal
773 246 (2014) 79–87. 10.1016/j.cej.2014.02.057.

774 [77] B. Polesso,, R. Duczinski,, F.L. Bernard,, H.Z. Ferrari,, F.D. Vecchia,, S.
775 Maria,, S. Einloft, Materials Research 22 (2019) 1–10.

776 [78] A. Aquino,, F. Bernard,, R. Ligabue,, M. Seferin,, V. V Chaban,, E.J.

Cabrita,, S. Einloft, Royal Society of Chemistry 5 (2015) 64220–7. 10.1039/c5ra07561k.

[79] K. Helene,, F. Rasmus,, R. Anders, 55(8) (2012) 1648–56. 10.1007/s11426-012-4683-x.

[80] V. Hiremath,, A.H. Jadhav,, H. Lee,, S. Kwon,, J. Gil, Chemical Engineering Journal 287 (2016) 602–17. 10.1016/j.cej.2015.11.075.

[81] F. Lagarde,, H. Srour,, N. Berthet,, N. Oueslati,, B. Bousquet,, A. Nunes,, A. Martinez,, V. Dufaud, Journal of CO2 Utilization 34(June) (2019) 34–9. 10.1016/j.jcou.2019.05.023.

[82] S. Zhang,, Q. Wang,, P. Puthiaraj,, W.S. Ahn, Journal of CO2 Utilization 34(June) (2019) 395–403. 10.1016/j.jcou.2019.07.035.

[83] F. Nakibuule,, S.A. Nyanzi,, I. Oshchapovsky,, O.F. Wendt,, E. Tebandeke, BMC Chemistry 14 (2020) 1–14. 10.1186/s13065-020-00713-2.

[84] Y. Kuwahara,, H. Yamashita, Biochemical Pharmacology 1 (2013) 50–9. 10.1016/j.jcou.2013.03.001.

[85] S. Verma,, R.I. Kureshy,, T. Roy,, M. Kumar,, A. Das,, N.H. Khan,, S.H.R. Abdi,, H.C. Bajaj, Catalysis Communications 61 (2015) 78–82. 10.1016/j.catcom.2014.12.013.

[86] Y. Kuwahara,, K. Tsuji,, T. Ohmichi,, T. Kamegawa, ChemSusChem 5 (2012) 1523–32. 10.1002/cssc.201100814.

[87] S. Fujita,, B.M. Bhanage,, Y. Ikushima,, M. Shirai,, K. Torii, Catalysis Letters 79(April) (2002) 95–8. 1011-372X/02/0400-0095/0.